ISSN: 2639-7455

Research Article

Earth & Environmental Science Research & Reviews

Gravitation Dynamics for (Paleo) Climate and Its Dynamic Environment

Zhiren Wang

Institute of Marine and Coastal Sciences, Rutgers, The State University of New Jersey

***Corresponding author**
Zhiren Wang, Institute of Marine and Coastal Sciences, Rutgers, The State University of New Jersey, 71 Dudley Road, New Brunswick, NJ 08901; Email: joewwh77@gmail.com

Submitted: 10 Jan 2019; **Accepted**: 17 Jan 2019; **Published**: 11 Feb 2019

Climate dynamics is meeting the barrier of complicated nonlinearity and limitation in methods and interdisciplinary development. Attempting to break through the barrier by working on this project for over 20 years, without a funding but with publication difficulties, I established gravitation dynamics that nonlinearly and cumulatively drives geophysical fluids to produce the observed climate-paleoclimate variations and meridian structure of circulations, adjust El Niño-La Niña cycles, and initiate and maintain planetary rotations without which the Earth would be different and Earth's climate would be chaotic. Gravitation dynamics may explain more climatic and astronomical phenomena such as the broad spectrum, asymmetry and stability of climate, two-wave zonal structure, El Niño significance within different oceans, Earth's heat maintenance, rotational difference of solar planets and Earth's Moon that should have no rich fluid, and more. Applications of gravitation dynamics are expected to improve climate prediction and the study of climate and its dynamic environment that includes the atmosphere, physical oceans, magma, and orbital drivers.

Sun-Moon gravitation (SMG) produces tides that dissipate their energy in oceans and solid Earth [1-3]. Separating SMG into tidal constituents and using harmonic analyses, tide-associated climate studies have found that frictional mechanisms produce residual circulations, create new harmonic constituents at frequencies different from those present in disturbing forces, and distort tides in shallow water regions [4-8]. However, "Eulerian tide-induced residual current is only a mathematical description of the transient eddy and has no physical reality because it is the result of the averaging process of transient phenomena", and the tide-associated climate studies are being challenged by the disciplinary complexity [9]. E.g., SMG-Eulerian dilemmas (explained in the Methods section) had failed us in seeing the accurate climatic effects from SMG, based on my studies of the gravitation-driven motion (GDM) of geophysical fluids [10-12].

The enchanting secret is the climate-paleoclimate variations with a broad-spectrum of periods of 40−50 days, 1−2 years, interannual and decadal variabilities, 1−2 ky, 23 ky, 41 ky and 100 ky [13-19]. For causes of interannual variability that is a prominent climate signal, studies have enlightened us in the views of westerly wind bursts, Kelvin and Rossby waves, Oscillations, self-sustaining internal dynamics, and stochastic forcing [20-26]. The causes of paleoclimate variations have been ascribed to insolation changing with eccentricities, obliquity and precession of the Earth's orbit, greenhouse forceings and stochastic resonance [18-31]. As reported in Sections 1 and 3, climate rhythm was enriched during the interaction between the active external SMG and the moving fluids, displaying the broad spectrum of climate-paleoclimate variations, with the observed periods occurring with high probability and the inter annual-variability phase adjusted through active SMG.

General atmospheric circulations highly influence interannual signals of climate and correlates with the meridian structure of the circulations that has been ascribed to the distribution of pressure-zones [32]. On the other hand, pressure-zones respond to circulations and thermal processes. Equatorial oceanic currents are believed to be driven by winds and the balance of zonal pressure gradient force and flow acceleration [33]. According to Ekman theory that I summarized into Equation (15) in the Method section and data of the last three decades (from the Earth System Research Laboratory, www.esrl.noaa.gov/psd, and Aviso www.aviso.oceanobs.com), winds produced smaller (below 52%) equatorial south/north equatorial currents (SEC/NEC) than those observed, and the balance of zonal pressure gradient force and flow acceleration produced much larger (up to $10ms^{-1}$) equatorial counter currents (ECC) than those observed [12]. The SEC, NEC, ECC and equatorial winds are all quasi-zonal, but the quasi-zonal winds mainly transport water away from the equator. Therefore, equatorial currents must originate from drivers other than only winds. The largely ignored GDM matters to circulations in size, structure and temporal variations, as reported in Section 2.

As the important dynamic environmental factors and playing key roles in weather-climate systems, planetary rotations were studied for their cause and maintenance. Planets are born from the collapse of dense interstellar clouds [34]. Structure formation theories such as top-down theories and bottom-up theories suggest that the galaxy formation to occur as a result of tiny quantum fluctuations in the aftermath of the Big Bang*, with a premise of initial push [35-37]. My guess is that: The Big Bang, if any, should be from the explosion of the "Black Hole" that has extremely great mass and density, and increases its mass and density by catching more and more mass and lights. As the mass and density increase, the contained energy and pressure also increase until the explosion occur to produce the Big Bang. The Big Bang should come from and end the "Black Hole. In a sense, the origin and maintenance of planetary rotations are still puzzles. Where is maintaining angular momentum from? Why do the gas giants (i.e., Jupiter, Saturn, Neptune, and Uranus) rotate faster than do the terrestrial planets (i.e., Earth, Venus, Mars, and

Mercury)? Why does Uranus retrograde while its neighbor Jupiter progresses? Why does the Moon not rotate? Will the Earth rotate stably in order to maintain a favorable weather-climate system? Section 4 may help answer the questions.

Gravitation dynamics can also explain some other long-standing climate questions and may help improve our climate prediction and studies (Section 5).

Result

Gravitation Dynamics for Temporal Climate-Paleoclimate Variations

The GDM of geophysical fluids may present observed the climate variations and provide reproducible energy inside Earth with its power varying on paleoclimate time scales. A periodic and small SMG could produce frequency-abundant and prominent GDM while SMG drove moving fluids and accumulated momentum over different durations in a certain direction, determined by the orbital properties (e.g., obliquity, revolution periods, radius and rotation rate), the location and relative velocity of fluids, as demonstrated in Equations (35−37, 43−56) of[10] and Equations (1−2) of[11] . The periodicity of GDM, computed from Equations (47−58) of[10] and Equations (4−6) of[11] and depicted in Figure 1, demonstrated the following major characteristics comparable to observations:

1. GDM had a broad-spectrum of periods, the faster the flow speeds, the shorter the periods with the occurring-probability (OP) that was proportional to the period-ranges and Earth's rotational speed (without rotation, OP would be zero), but approximately inversely proportional to the total speed space and the square of the period length. OP was larger at lower latitudes than at higher latitudes (proportional to cos of latitudes).
2. The period of GDM was symmetrical for meridional flows, but asymmetrical for zonal flows especially for periods shorter than ten years (the shorter the periods, the more asymmetrical the periods were). For seasonal to interannual variations, the eastward speed space was significantly larger than the westward space for a given period range, suggesting that eastward flow tends to cause fluids to oscillate with greater ease than westward flows. In reality, large eastward wind anomalies often correspond to an unstable shift from a normal to an El Nino phase during an El Niño/Southern Oscillation (ENSO) cycle that are also zonally asymmetrical [32, 38]. An asymmetrical ENSO with a longer phase of La Niña may be further explained, in a sense, using the lasting westward GDM in low latitudes.
3. Each period of GDM corresponded to a specific present speed of u and v components. Shorter (e.g., seasonal to interannual) periods largely occurred in the atmosphere with faster flows, longer (e.g., quasi biennial oscillation, interannual and decadal) periods typically occurred in oceans with slower flows, much longer (e.g., 1-2ky and 20-150ky) periods typically occurred within magma. Averaged for latitudes, OP ≈ 86% or 0% for a 1 to 3-month oscillation if $-20 \le u \le 40 \cup -30 \le v \le 30$ *or* $-0.3 \le u \le 1.6 \cup -0.6 \le v \le 0.6$ m/s (∪ represents "and"), indicating that this oscillation mainly occurs within the atmosphere but rarely within oceans; OP ≈ 69% or 0% for a 1 to 3-year oscillation if $-2 \le u \le 4 \cup -3 \le v \le 3$ *or* $-0.2 \le u \le 0.2 \cup -0.2 \le v \le 0.2$ m/s, mainly occurring in the upper oceans of faster currents and in the atmosphere of slower winds; OP ≈ 54% or 0% for a 3 to 10-year oscillation if $-1 \le u \le 2 \cup -1.5 \le v \le 1.5$ or $-0.06 \le u \le 0.06 \cup -0.06 \le v \le 0.06$ m/s, mainly occurring in the atmosphere and oceans of slower flows; and OP ≈ 63% or 0% for a 10 to 20-year-oscillation if $-7.5 \le u \le 7.5 \cup -7.5 \le v \le 7.5$ *or* $-3 \le u \le 3 \cup -3 \le v \le 3$ cm/s, mainly occurring in the oceans of slow currents. The basic periodic component of a half month or a half year existed independent of the flow speed (OP =100%), contributing to the seasonality. OP ≈ 74%, 58%, and 69% for magma motions in periods of 1-5ky, 20-50ky, and 50-150ky if $-900 \le u \le 900 \cup -900 \le v \le 900$, $-45 \le u \le 45 \cup -45 \le v \le 45$, and $-5 \le u \le 15 \cup -15 \le v \le 15$ μm/s, respectively.

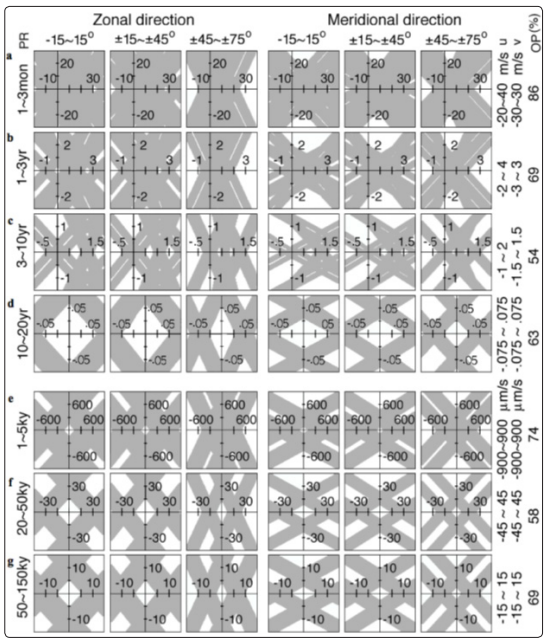

Figure 1: Occurrence for different periods of GDM. Period ranges of GDM (PR column, y-labels) and their occurring-probability (OP column averaged for columns 1-6, %) in different speed spaces (u-v speed components, set as abscissa-ordinate) for the atmosphere and oceans (m/s, **a, b, c** and **d**) and for magma in the lower mantle (μm/s, **e**, **f** and **g**. Columns 1-3 / 4-6 are the periodicity of zonal / meridional motion at the labeled latitudes (positive for the North Hemisphere). The OP is the ratio of the shaded u-v area where the PR occur to the total u-v area labeled on the "u" and "v" columns, computed using Equations in [11] and [12].

The paleoclimate variations were presented within the power of GDM (PGDM) in magma motion. For the past observed 800ky, PGDM produced similar spectra and phase distribution with those of observed temperature and CO_2 concentration (Figure 2), with periods of ~40 (38.79−41.27), ~80 (77.58−82.54), and ~100 (96.97−103.17) ky, with the total phase length much longer during negative anomaly phases than during positive anomaly phases (417 vs 383 ky), and with the amplitude much smaller during negative anomaly phases than during positive anomaly phases (1,210 vs 2,060 TW). Similarly, the spectra of both temperature and CO_2 displayed periods of ~40 (38.79−41.27), ~70 (67.88−72.22), and ~100 (96.97−103.17) ky, with much longer total phases during negative-anomaly phases than during positive-anomaly phases (443 vs 357 and 412 vs 389 ky), and with much smaller amplitudes during negative-anomaly phases than during positive-anomaly phases (5 vs 10°C and 52 vs 75 ppm). (1 TW=10^{12}W, period ranges were from error estimations via a chi-square test for a 95% significance level.) [39].

Temperature, CO_2 concentration, and PGDM yielded a slower

accumulation during the longer negative anomaly phases, but a relatively quick release during shorter positive anomaly phases. Insolation (Milankovitch Cycles) that summarizes most thermodynamics of active orbital forcing has no the slow-accumulation and quick-release character, but has slightly shorter total phase and weaker amplitude during negative-anomaly phases than during positive-anomaly phases (391vs 409 ky and 63 vs 66 Wm^{-2}), and yields a low correlation (~24.9%, at a 95% confidence level using a t-test, same for all the correlations mentioned below) to temperature over the past 800 ky [11].

PGDM may be significant in paleo climate variations and Earth's heat budget. Magma, located beneath Earth's shell, has a mass approximately 3,400 times of the mass of the atmosphere plus oceans. Earth's shell covered with the atmosphere concentrated within the troposphere and oceans are like a thin layers floating above and being heated by magma. Although solar radiation hardly heats the inner Earth, PGDM may provide reproducible energy to maintain an energetic inner Earth by compensating for Earth's heat loss (Earth's collapse, formation, cooling, and radioactivity all are incurring the decay and heat loss of Earth) [40-42].

Depending on the magma speed and dissipation, PGDM could have a standard deviation of ~500 to 7,000 TW, or ~0.98 to 13.7 W per square meter of Earth's surface, more than heat flowing through the seafloor from the lower lithosphere (~32 TW), heat flux increased from anthropogenic greenhouse gases (0.85 ± 0.15 W per square meter of Earth's surface), and the total Earth heat budget (~41 TW) approximately 54% of which cannot be balanced [42-44].

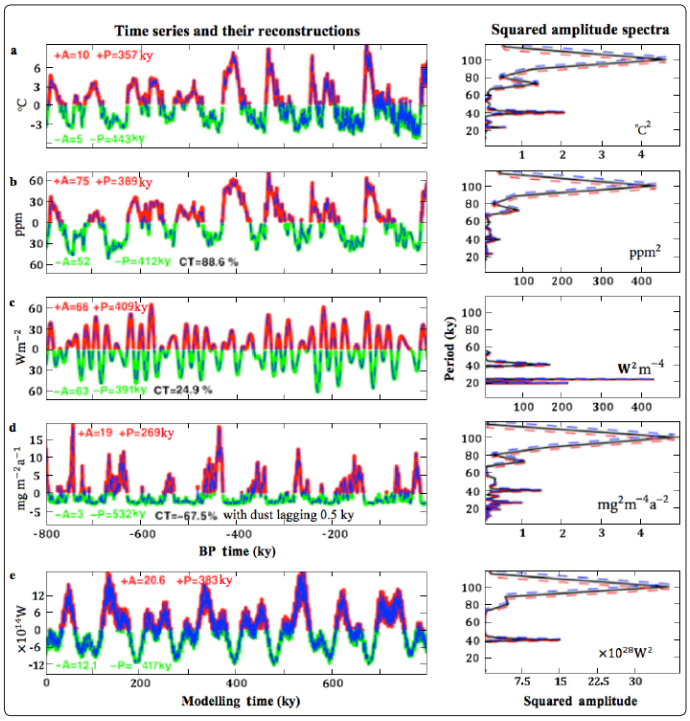

Figure 2: Time series with mean deducted (left, data interval is 0.1ky) and its squared amplitude spectrum (right) for a, temperature, b, CO2, c, insolation (Milankovitch cycle), d, dust from the EPICA Ice Core during July at 65°N for the past 800ky, and e, total PGDM (using cf = $0.001s^{-1}$, *uq*, *vq* = 2.4 and 4 μm/s for the lower mantle and outer core, respectively, see Methods section). Time series (red-green curve) were 100% correlated to their reconstructions (dashed blue curve) that were produced via my squared-speed spectrum analysis, and were evaluated using the positive/negative amplitude (+A/-A), total phase length for positive/negative phases (+P/-P), and correlation to the temperature (CT) [24]. For the spectra (black curve), errors (dashed blue/red line for the upper/lower limit) were estimated via a chi-square test for a 95% significance [51-52].

Could PGDM influence paleoclimatic variations through CO_2 and methane release by heating Earth, slow heat-transport, or sporadic heat-eruptions during magma convection? The shallow Arctic shelves are the main supplier of methane. A 3-degree increase in the Earth's surface temperature may release significant methane and CO_2 into the atmosphere. The shelf rise and horizontal stretching of the upper permafrost horizons may produce cracks to leak methane and CO_2 from below [45]. Over the past 800 ky, CO_2 and dust were highly correlated (0.89 and -0.68, respectively, Figure 2) to temperatures, and their slow accumulation and fast release sound like eruptions. Dust concentration in the atmosphere lagged temperature by approximately 500 years, implying that before eruptions to add dust into the atmosphere, magma may have begun to heat the atmosphere, followed with dust eruptions to cool the atmosphere through blocking solar radiations. Accumulating the energy (~10^{17} J) released during the eruption of Mount St. Helens in May 1980 [46]. Would take ~6 hours with the heat from a 500 TW of PGDM. Eruptions would occur too frequently due to PGDM release without slow heat release across Earth's surface.

Gravitation dynamics for meridian structure and temporal variations of circulations

Meridian structure of GDM for circulations

Figure 3 depicts the meridian structure of GDM based on Equations (1) and (2) for different Initial speeds, integrated with time steps of 6 − 600s and dissipation coefficients of 3×10^{-9}–120×10^{-9} s^{-1} for the atmosphere, and with a time step of 240 s and dissipation coefficients of 10^{-8}–10^{-6} s^{-1} for the Pacific and Atlantic Oceans between latitudes of 60°S and 60°N (non western-eastern horizontal boundaries employed). Nearly independent of time steps and dissipation coefficients, similar meridian structures of GDM were obtained, as characterized below.

Within the atmosphere, approximately 4 − 8.8% SMG was applied efficiently on the momentum accumulation. To reach a significant GDM (e.g., of 20 m/s), the maximum acceleration would have to act on fluids for a few seasons (~145 days); while the typical time interval required to accumulate the significant GDM was approximately on an interannual time scale (four to seven years around latitudes of ±35° and ±65° and nine to ten years at other latitudes). With the strong eastward flows (e.g., of 20 m/s), momentum accumulated much faster at latitudes of 30 ±5°, and the typical time interval required to accumulate the significant GDM could be shorter (two years). After accumulating for approximately four years within oceans, GDM will reach a speed of approximately 3 m/s. A stable meridian structure of zonal GDM was maintained, nearly independent of initial currents. The time scales for momentum accumulation match circulation adjustment for seasonal to inter annual variations (see Section 3 for details).

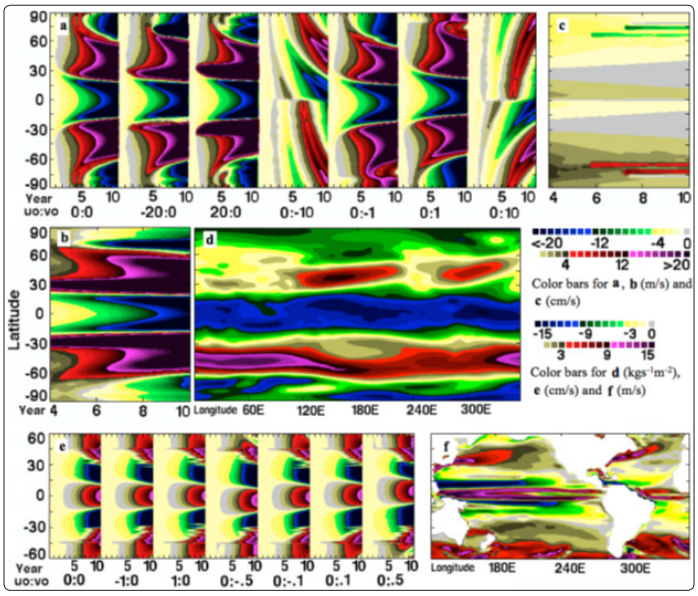

Figure 3: Structural GDM accumulated for the atmosphere (**a** and **b** for u component and **c** for v component) and Pacific-Atlantic oceans (e for u component) against time (x-axis) and latitude (y-axis) at different initial u:v speeds (m/s, x-axis uo:vo), computed using Equations in [11] and [12]. b and c were averaged for all the initial speeds as listed in **a**. **d**, observed atmospheric zonal mass flux (wind times density) averaged from 1980-09 and within 100-1,000hPa. **f**, observed oceanic currents averaged from 1980-2009 and within a depth of 0-225m. Data were obtained from the Physical Sciences Division, Earth System Research Laboratory.

Within the atmosphere, the long-term GDM was of a quasi-zonal character with the zonal component much greater than the meridional component. The meridional component went toward the equator (pointing toward the point-blank latitude), which is described in Equation (2) and may contribute to westward motion at lower latitudes under a rotational Earth. The mean zonal GDM was easterly in low latitudes from approximately 19±2°S to 19±2°N, westerly in the mid-latitudes from approximately 19±2°S/N to 63±12°S/N, and easterly in latitudes higher than approximately 63±12°S/N, which was structurally consistent with observations. Observed atmospheric mass flux (wind times air density) was easterly in low latitudes from approximately 17.5°S to 17.5°N, westerly in mid-latitudes from approximately 17.5°S/N to 70°S/N, and easterly in latitudes higher than approximately 70°S/N.

Within the Pacific and Atlantic oceans, mean zonal GDM was eastward within equatorial zones of approximately 10°S−10°N, westward within 10°S/N− 30°S/N, and eastward within 30°S/N−60°S/N. The mean zonal GDM is comparable to the mean Pacific and Atlantic zonal currents that are eastward within equatorial zones of 4°S−10°N (extendible to 10°S near western and eastern Pacific Ocean), westward within 10°N−30°N, 4−10°S and 21−39°S, and eastward within 30°N−60°N and 21−60°S. However, differences in structure and size existed between GDM and observation because western-eastern horizontal boundaries were not included here and wind-driven currents as well as thermohaline make different.

For both the atmosphere and oceans, meridian structure of GDM was eventually maintained and could be established either from the static or moving flows. Zonal winds and currents were much smaller than Earth's rotational speed (i.e., $|u| << 460 \cos \varphi$, φ is latitude) and, therefore, had little affect on the structure of GDM except near poles where the structure of GDM varied with the initial zonal speed and temporal scales, and where the actual weather-climate systems also varied considerably. From a dynamic view, the stable and unceasing momentum accumulation of GDM at different latitudes may dynamically contribute to maintaining a certain meridian circulation structure and a stable climate. The low-latitude westward GDM may have initiated the warm pool in the joint Indian-Pacific region by transporting warmer surface water toward western horizontal boundaries, starting the thermal Walker circulation. Persistent low-latitude westward GDM helps maintain ENSO cycle with a longer normal phase and La Niña-like patterns of ENSO, which was the case for the past half century [32].

Temporal variations and significance of GDM for equatorial currents

Linearly estimated GDM partially explained and correlated to NEC, SEC and ECC variations (GDM-current correlation was 33%−48%) and produced significant fluxes [12].Off-equator, Equator-ward SMG produced westward currents, linearly estimated as -1−-2/-2−-6 mm/s under the gravitation of the Sun/Moon, or on average -20.8 Sv (1Sv=10^6 m^3/s) across a section of 0−2000m depth and 10°S/N−20°S/N (the observed SEC plus NEC produces a flux of approximately -28.7 Sv). Near-equator, SMG-driven ECC was approximately 5−8/14−16 mm/s under the gravitation of the Sun/Moon within 5°S−5°N, or on average 19 Sv within a depth of 0−500m (the observed ECC produces a flux of approximately 20 Sv).

Gravitation dynamics and phase adjustment during ENSO cycles

Proofs from observations

Phase-adjustment mechanism is the key for the study and prediction of an ENSO cycle. Based on modeling and data of sea-surface temperature (SST) averaged within Niño3.4 region, atmospheric and oceanic circulations averaged at surface and within equatorial Pacific Ocean during the period of 1980 − 2007 (data were from the Physical Sciences Division: www.esrl.noaa.gov/psd), responsive processes within the atmosphere and oceans (e.g., westerly wind bursts, noises) can not adjust phase and guarantee the seasonality of ENSO, but are often temporarily concomitant with circulations. El Niño often accompanies with a weakened and eastward retreated Walker circulation and an eastward zonal wind anomaly, while La Niña often accompanies with an intensified and westward extending Walker circulation and a westward zonal wind anomaly. Zonal wind/current and its acceleration were correlated to SST with correlations of 0.85/0.57 and 0.8/0.35, respectively. A positive/negative anomaly of the zonal wind helps establish a convergent/divergent in the east equatorial upper Pacific Ocean to increase/decrease the SST there [12, 32]. Where are the accelerations from to produce wind anomalies? A small fraction of the available potential energy is often established and released for the quick weather processes and does not guarantee the seasonality and interannual signal embed in ENSO cycles [47]. Wind-driven currents lags winds and goes at different directions. That the meridional accelerations of winds and currents highly correlate with a simultaneous correlation of 0.95/0.96 within low latitudes [12]. Implies that winds and currents share the same external dynamic forcing that should be the SMG applying on the atmosphere and oceans and producing ENSO-feedback tendencies [12].

SMG-driven seasonal and interannual ENSO-feedback tendencies

SMG-driven acceleration actively changed the present flow speeds and caused phase adjustment in an ENSO cycle, depending on orbital parameters and present flow speeds, as defined in Equations 3.75 and 3.76 (See [12] for details. A positive/negative zonal SMG-driven acceleration had eastward/westward flow feedback tendency, weakened the present westward/eastward flow to produce negative zonal feedback tendency, or enhanced the present eastward/westward flow to produce positive zonal feedback tendency. As depicted in Figure 4, all feedback tendencies were symmetrical for the present meridional flows with peak values occurring when the present meridional flow speed was zero, were unsymmetrical for the present zonal flow, were significant in May to June, changed with the present zonal flows (e.g., became weak and uncertain for zonal present winds around -20, -1.0, 0, 1.0, or 15 m/s, and enhanced for the present current around -0.125m/s), conduced to transferring to or maintaining a La Niña or an El Niño phase, and transferred from one tendency to another one if, e.g., the present zonal wind was <-20 m/s for winds, <-0.9 or >0.6 m/s for currents, based on examinations for a four-year period, different present flow speeds, multiple initial relative longitudes and phases of the Sun and Moon.

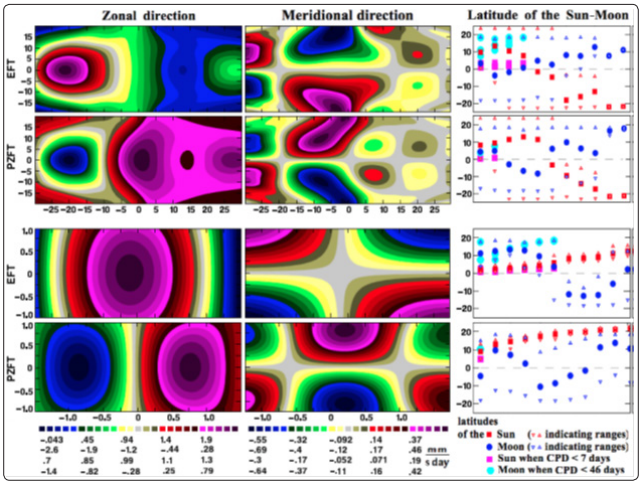

Figure 4: Different feedback tendencies (columns 1−2) of SMG-driven winds (rows 1−2) and currents (rows 3−4), with x-axis and y-axis representing the present zonal and meridional flow speeds (m/s), and the latitudes of the Sun and Moon during the feedback tendencies (column 3). EFT: Eastward flow feedback tendency (figures are identical to westward flow feedback tendency but with opposite signs). PZFT: Positive zonal feedback tendency (figure is identical to negative zonal feedback tendency but with opposite signs). CPD: phase difference between atmospheric and oceanic circulations.

Within the four-year period, a timing-overlap of positive/negative zonal feedback tendency in both atmospheric and oceanic circulations occurred for only a couple times in March to April when the Sun/Moon located at latitudes of 0.4−4.8° N/3.8−10.1° N, with the Sun's phase difference between atmospheric and oceanic circulations no more than one and half months. And all the feedback tendencies occurred when the Sun and Moon were located over the Northern Hemisphere. This displayed a clear seasonality, interannual variation, and temporal asymmetry for the short-range climate system.

A small change in circulations can transport huge amount of energy and may cause weather-climate adjustment. On average, 0.2−1.0 m/s (0.2−2.0 cm/s) of zonal wind (current) anomaly occurred during El Niño phases, and SMG-driven acceleration could be 1. 5 −2 mm/s/week for the atmosphere and 0.5−1.5 mm/s/week for oceans. Accordingly, the adjusting time to cancel out the zonal wind (current) anomaly is estimated as approximately 2−10 years (2−40 weeks) within the atmosphere (oceans), implying that oceanic circulations can be adjusted much faster than atmospheric circulations seasonally and interannually.

Gravitation dynamics for the origin and maintenance of planetary rotations

The phenomenon for planetary rotation are interesting, e.g., Uranus retrograde while Jupiter progresses although they are neighboring, and the gas giants rotate significantly faster than the terrestrial planets although the gas giants have much larger momentum of inertia and are remoter to the Sun than the terrestrial planets (See Table 1 for details). Dynamically, planetary rotation is playing roles of maintaining our weather-climate system, as partially listed below.

1. All inertia waves and motions within geophysical fluids require Earth's rotation that produces quasi-geostrophic motions and keeps orderly and lasting fluid motions by making fluids mostly move along isobars (without Earth's rotation, fluids would immediately move from high to low pressures) [12].
2. In addition to distributing solar radiation to all sides of Earth, stable Earth's rotation may have balancing effect on horizontal and vertical motions in order to make geophysical fluids evenly distributed to form planetary shape of a sphere or an ellipsoid by keeping fluids from heaping or losing to a fixed attraction direction. Since flow on the Moon would not be evenly distributed without a rotation, a reason may exist as to why no uniformly or richly distributed fluid(s) exist on the non-rotational Moon. Without Earth's rotation, vertical GDM would increase by approximately 365 and 29 times under the gravitation of the Sun and Moon, respectively, estimated using formula (parameters were described in Method section) [12].

$$\sqrt{[(2f_e - 2f_{ir} + 2VR_e^{-1})^2 + k_f^2]/[(-2f_{ir} + 2VR_e^{-1})^2 + k_f^2]} \approx f_e/f_{ir}$$

For solids or fluids having an extremely large viscosity (kf is extremely large, the above ratio is 1), the balancing effect will disappear.

3. Earth's rotation helps geophysical fluids memorize SMG momentum input and accumulate momentum to produce orderly circulations in multiple periods, as reported above.
4. Earth's rotation produces the Coriolis force that balances most of the gradient force and dwarfs the nonlinear advection term in kinetic equations, and help increase the predictability of weather-climate system. Etc.

Here, I reported that the nonlinear motions of geophysical fluids under the external gravitation of celestial bodies produced the accumulative angular momentum that initialized and maintained planetary rotations.

Rotations of Earth, Mercury, Jupiter and Uranus

Fluids (i.e., gases and liquids) dominated the original hot Earth, providing the rotational materials for Earth under SMG [34]. For their GDM produced a net eastward zonal angular momentum that could have initiated Earth's rotation, the higher percentage of fluids,

the faster the Earth rotated, based on computation using GDM under the changing Earth in density, radius, different percentage of available fluids and their viscosity (Equations (1−8) in the Method section, depicted in Figure5). Time step was set as 30 minutes (multiple time steps produced similar results), and Earth's entire thickness was separated into 50 layers for numerical computation. Beginning with a zero initial rotation rate (no initial rotation was required for GDM to initiate Earth's rotation, as long as fluids existed), the original Earth began to rotate eastward with a net GDM-induced eastward zonal angular momentum. Earth's rotation accelerated at the beginning for a period of time with a reduced Earth's size and, therefore, its moment of inertia as Earth cooled down. Then the rotation speed increased slowly and eventually approached stabilization as Earth cooled down, available fluids were reduced and their viscosity increased with decreased temperatures. For the tested Earth's cooling rate, an increase in rotation rate from zero to approximately 2.51×10^{-6} s^{-1} (~3.5% of the modern rate) could have occurred in ~1,000 years, and under Earth's "recent" conditions [34] the rotation rate could have increased from 6.56×10^{-5} s^{-1} (~90 % of the modern rate) to the modern rate in approximately 50-100 years. As rotation approaching its modern rate of 7.27×10^{-5} s^{-1}, Earth rotated stably with less input of the angular momentum provided by less available fluids. Since the rotation rate changed very little after Earth reached its current rate, the modern rotation rate appeared to be the stable limit for modern conditions.

Mercury, Jupiter and Uranus may rotate with the same mechanism as Earth, driven by the Sun, planets and their moon(s). Planets containing higher percentage of fluids rotated faster, and this is the case for the solar planets. The gas giants contain higher percentage of fluids and rotate faster than the terrestrial planets do. Experiments were performed for Mercury, Jupiter and Uranus for a time period of hundred years, with only the Sun employed to produce GDM. Time step was set as 30 minutes, and their entire thickness was separated into 50 layers for numerical computation. Beginning with a zero initial rotation rate, the original Mercury, Jupiter and Uranus began to rotate with a net GDM-induced zonal angular momentum. As it is observed in rotation directions, Mercury rotated eastward (progressed) at a larger acceleration at the beginning ten years and then the rotation rate increased slowly, Jupiter rotated eastward (progressed), and Uranus rotated westward (retrograded). Uranus has a much larger obliquity (~97.8°) than Mercury, Earth and Jupiter. If Uranus had the same obliquity as Jupiter (~1.3°), Uranus would rotate eastward (progressed), but the rotation would oscillate much, likely due to this "unmatchable" obliquity, implying that the obliquity of the orbit of Uranus determined Uranus's rotation direction.

Mechanism of planetary rotation and its implications

The rotation mechanism of Earth, Mercury, Jupiter and Uranus can be summarized as: Under the external gravitation of celestial body or bodies, fluids contained in a planet can accumulate angular momentum and cause the planet to rotate. The higher percentage of fluids contained in a planet, the faster the planet rotate, depending on orbital properties such as obliquity that may determine rotation direction. This mechanism is consistent with and supported by what we understand about Earth's Moon and the eight solar planets (Table 1), among which the four gas giants containing more fluids rotate much faster than the four terrestrial planets of less fluids.

Based on this mechanism, it is logical to reason that no uniformly or richly distributed fluid(s) should exist in the non-rotational Moon. Otherwise, under the gravitation of the Sun and Earth, fluid(s) would cause the Moon to rotate. If the Moon once rotated at an initial rate, without fluids it would cease to rotate due to dissipation of its angular momentum. Virtually no water or other volatiles have been found on the Moon, or the Moon originated after a body struck the proto-Earth, or it was once a part of Earth that spun off after a giant collision with another body [48-49]. That Mars rotates in a manner similar to Earth likely supporting the existence of fluid(s), that Venus retrogrades at a much slower rotation rate (approximately 1/240 of Earth's rotation rate) might imply that less fluids exist in Venus, and that Mercury of a much smaller moment of inertia rotates much more slowly than Earth might imply that even less fluid(s) exist in Mercury [50].

Table 1: The rotation properties of the solar planets associated with fluids [50].

Solar planet	Sidereal rotation rate (rad/s)	Moment of inertia (kg m^2)	Orbit radius (m)	State (solid, fluid)
Jupiter	1.76×10^{-4}	2.36×10^{42}	7.786×10^{11}	Gas giant composed mainly of hydrogen and helium
Saturn	1.64×10^{-4}	4.34×10^{41}	1.433×10^{12}	Gas giant composed mainly of hydrogen and helium
Neptune	1.08×10^{-4}	1.82×10^{40}	4.503×10^{12}	Gas giant composed mainly of hydrogen, helium and ices
Uranus	1.01×10^{-4}	1.30×10^{40}	2.877×10^{12}	Gas giant composed mainly of hydrogen, helium and ices
Earth	7.27×10^{-5}	8.04×10^{37}	1.496×10^{11}	Terrestrial planet primarily composed of rock, metal, air and water
Venus	-2.99×10^{-7} (retrograde)	5.88×10^{37}	1.082×10^{11}	Terrestrial planet primarily composed of rock and metal Any fluid?
Mars	7.09×10^{-5}	2.70×10^{36}	2.279×10^{11}	Terrestrial planet primarily composed of rock, metal andwater ice Any fluid?
Mercury	1.24×10^{-6}	6.49×10^{35}	5.791×10^{10}	Terrestrial planet primarily composed of rock and metal Any fluid?

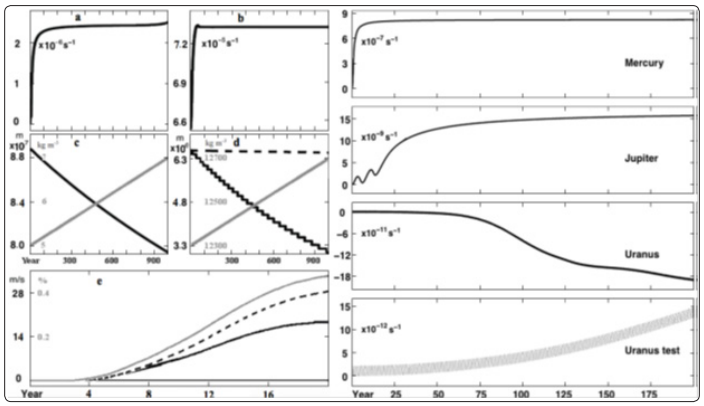

Figure 5: GDM-driven planetary rotation. **a**, Earth beginning with a gaseous state, a zero initial rotation rate, with a changing Earth's radius (black) and density of Earth's core (gray) in **c**. **b**, Earth beginning at 90% of its modern rotation rate and cooling for 1,000 years before approaching modern state, with Earth's radius (black, dashed), core density (gray), and fluid radius (black, solid) in **d**. **e**, GDM-driven net meridional momentum, angular momentum of the atmosphere plus oceans (black), zonal angular momentum of the atmosphere (blue) and oceans (green), and the rotation contribution to modern Earth's rotation rate (red). All angular momentum was divided by Earth's radius and for per unit mass. (Right column) Rotations of Mercury, Jupiter and Uranus within the beginning two hundreds of years. Mercury, Jupiter and Uranus started at a gaseous state and a zero initial rotation rate. The last row is for an experimental case for Uranus but using the obliquity of Jupiter. Computation was performed using equations (1) to (10).

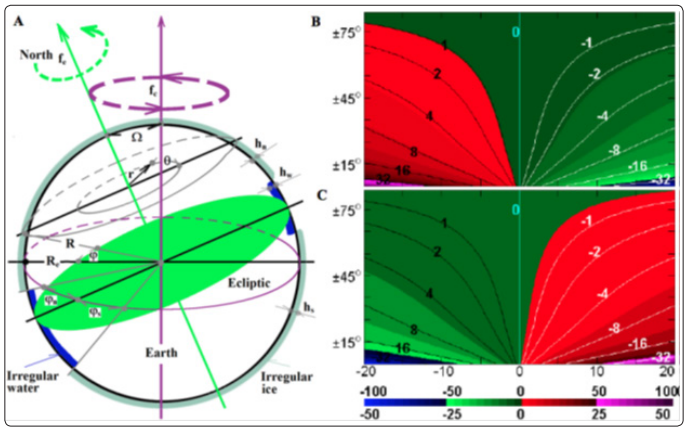

Figure 6: Changes of Earth's rotation, obliquity and inertia momentum. Model diagram **(A)**: $\mathbf{h_w}$ is the thickness of irregularly formed water within latitudes of $\boldsymbol{\varphi_s}$–$\boldsymbol{\varphi_n}$, $\mathbf{h_n}$/$\mathbf{h_s}$ the thickness of irregularly formed ice within latitudes other than $\boldsymbol{\varphi_s}$–$\boldsymbol{\varphi_n}$, Re (R) Earth's normal (changed) radius, $\boldsymbol{\varphi}$ the latitude angle, $\mathbf{f_e}$ and $\mathbf{f_c}$ the Earth's rotation rates circling Earth's axis and the axis perpendicular to the Ecliptic, respectively, and **Ω** Earth's obliquity. Modeling results: (B) Earth's obliquity ($\times 10^{-2}$ degree, using scales above the color bar) and (C) Earth's rotational angular speed ($\times 10^{-8}$ rad/s, using scales beneath the color bar) as well as Earth's inertia momentum ($\times 10^{34}$ kg m^2, isolines), computed from Equations (11) to (14). X-axis is the thickness (km) of irregularly formed ice, y-axis the ice-edge latitude (degree, positive/negative for the Northern/Southern Hemisphere). Irregularly formed ice covered regions from ice-edge latitudes to the pole within one hemisphere and water within the remaining regions correspondingly reduced under mass conservation.

Maintenance of stable Earth's rotation

Although rotating fast at a rate up to ~460 m/s, Earth is rotating stably for reasons:

1. For the current Earth system, GDM of the atmosphere and oceans provided nearly zero net meridional angular momentum, but a persistent eastward net angular momentum to maintain stable Earth's rotation during balanced by factors including friction dissipation.
2. Rotation itself never incurs the consumption of the rotating momentum because it never works on moving objects whose speed is always perpendicular to Coriolis force.
3. The much greater Earth's radius and momentum of inertia relative to their changes helped stabilize Earth's rotation by muffling interruptions. Fluids may change Earth's obliquity, inertia momentum and rotation rate, but very little. The most significant event may be the irregular mass distribution related to extreme climate. An exaggerated uneven distribution of surface water was checked here via my model described in Figure 6 and Equations (11-14) in the Method section: Suppose ice was irregularly formed with a thickness up to 20 km, covered various regions from Different edge-latitudes to a pole, and concentrated within only one hemisphere. Modeling results are depicted in Figure 6. The exaggerated increased (reduced) ice would reduce (increase) earth's obliquity, inertia momentum and rotation rate very little, no more than 1o (~4% of the modern obliquity) 5.5×10^{35} kg m^2 (~0.7% of the modern inertia momentum), and 5×10^{-7} s^{-1} (~0.7% of the modern rotation rate), respectively. The much greater Earth's radius and momentum of inertia relative to their change helped stabilize Earth's rotation by muffling interruptions.

Gravitation dynamics for improving our climate prediction and study

As reported in my published book, gravitation-dynamics could also explain some other long-standing climate questions such as: Explanation for two-wave structure: SMG itself presented the basic climatic wave characteristics of a two-wave structure along latitude parallels, fast westward-propagating and slow eastward-propagating, likely serving as the trigger factors for the observed fast westward-propagating Rossby wave and slow eastward-propagating Kelvin wave [12]. Explanation for ENSO significance and Kuroshio: For the whole depth of tropical oceans, SMG was the major vorticity source (2−4 times of that provided by wind stress that drives upper oceans). The two-wave structure of SMG along latitude parallels produced different oscillation intensities, 1.5−2 times stronger in Pacific Ocean whose size covers peak SMG waves than Atlantic and Indian Oceans whose sizes cover partial SMG waves. Significant fluxes could be produced from GDM within a large cross section. Compared to west shelves of the Indian and Atlantic Oceans, the larger area and slower slope of west shelf of the Pacific Ocean intensified the GDM flows on it within 2° S − 10°N where the Kuroshio is located, producing western intensification. Depending on the Earth's radius (R_e), thickness (H) of water column, and slope (Sx) of shelf, SMG-driven shelf currents could be amplified by HS_x^{-1} R_e^{-1} times, maximum within the west Pacific Ocean.

Gravitation dynamics may contribute to the study and prediction of weather and climate. Current climate models can hind cast historical climate patterns well over long periods because they are driven by observed variables that already included the frequencies and structures of climate factors such as winds and

the accumulated momentum from GDM. Adjustable parameters are often indispensable for better modeling effects. However, in predicting windows without accumulated momentum from GDM counted in, prediction uncertainties come up soon and increase with prediction length, coming up so soon that the nonlinear dynamics may be a larger "suspicion" for causing them than the mostly linear thermodynamics. Introducing gravitation dynamics with solved "SMG-Eulerian dilemmas" and fine resolutions as well as new discretization methods may help for better understanding of weather-climate dynamics and its environment that not only includes the atmosphere and oceans, but is also extended into geological factors (e.g., magma motion and Earth's heat), astronomic drivers (e.g. the Sun-Moon attraction and planetary rotation), and their combination [12].

Methods

Scale-analysis method that omits small-magnitude SMG is about applicably for linear processes and short-term weather systems where the quasigeostrophic processes define the first mode of fluid motions. For climate within a large space and a long time duration, small SMG accumulatively and nonlinearly drives geophysical fluids to produce second mode of fluid motions that may add into the real circulations and change circulation structure and energy transport. Perhaps, SMG was not too great to leave room for weather processes and not too small to maintain climate background from chaotic state.

Due to high-resolution requirements and mathematical complexity, numerically understanding the cumulative effects on climate within Eulerian frame is still difficult. SMG changes with the relative locations between fluids and the Sun or Moon. In order for a numerical model to determine the changing locations of fluids, grid spacing must be smaller than the distance for fluids to move within one-time step in the discrete Eulerian system. The longer the temporal scale needed to study or predict, the smaller the speed that dynamically contributes to the corresponding temporal variation, indicating that a higher resolution is required for a longer-term climatic model [10]. In order to catch the accurate relative locations between fluids and the Sun or Moon, the fast Earth rotation makes the time step much shorter than that used by classic climate models. If, for example, the time step is 1 minute and the smallest speed that needs to be simulated is 0.05m/s (typically for the variation of ~10 years), grid spacing must be smaller than 3m. Increasing time step may enlarge the grid spacing, but will result in error for the relative locations and miss the momentum cumulative effect [10]. Here comes the "SMG-Eulerian dilemmas" that are summarized as:

1. Longer-term climate modeling uses lower spatial resolutions and longer time steps to meet the well-posedness for a numerical solution and computation limitation, which, however, is contrary to the requirement for solving GDM: much higher spatial resolutions and shorter time steps are required in order to pinpoint the relative locations between fluids and the Sun or Moon due to the fast Earth's rotation and slower flow speeds for longer-term climate signals [10].
2. Mathematical misrepresentation and linearization exist during numerical modeling that transfers Newton momentum equation written in Lagrangian system into that written in a discrete Eulerian system, firstly as $\partial \boldsymbol{V}/\partial t + (\partial \boldsymbol{V}/\partial t) = \boldsymbol{F}$, then discretized as $\Delta_t \boldsymbol{V}/\Delta t + (\Delta s \boldsymbol{V}/\Delta s)\, \Delta s/\Delta t = \boldsymbol{F}$. ($\boldsymbol{V}$ is the speed of fluids, whose size is $|\boldsymbol{V}|$, $\boldsymbol{F}$ is an external force, s and t are spatial and temporal coordinates, respectively, Δs is the distance for the local fluid to move within one time step Δt , $\Delta_t \boldsymbol{V}$ and $\Delta_s \boldsymbol{V}$ are the increments of $\boldsymbol{V}$ within Δt and Δs, respectively.)

There are two mathematical preconditions for the discretization to be correct, i.e., $|\boldsymbol{V}| \equiv \Delta s/\Delta t$ and $\Delta s \equiv \int_t^{t+\Delta t} |\boldsymbol{V}| dt$. For nonlinear fluids, however, these preconditions were not met, because Δs was not the grid spacing ΔL, but the distance for the local fluid to move within one time step, and |V| is not always constant within $[t, t + \Delta t]$ (the mean state within a discretization grid was used to replace the state at one point). Normally $\Delta L >> \Delta s$, and the real gradient at local points can be much greater than that averaged within the grid spacing. However, "$\Delta s \equiv \Delta L$ and V=constant within $[t, t + \Delta t]$" are always applied in the real numerical modeling, which causes unavoidable mathematical misrepresentation and linearization that may be worsened by smoothing, filtering and parameterized mixings.

Here, in order to avoid the SMG-Eulerian dilemmas and to perform a preliminary study of the GDM of geophysical fluids that are defined to include not only the atmosphere and oceans, and Magma as well, a simplified dynamical model was set in a geostrophic environment and expressed within the Lagrangian, using local coordinates, as follows:

$$\frac{du}{dt} = V_o f_e sin\phi - \frac{1}{\rho}\frac{\partial p}{\partial x} - k_f u - \sum_{i=m}^{s} \frac{g_{io}}{4} \sum_{j=1}^{6} A_j \sin(q_{uj} t + X_j) \quad (1)$$

$$\frac{dv}{dt} = -V_o f_e sin\phi - \frac{1}{\rho}\frac{\partial p}{\partial y} - k_f v + \sum_{i=m}^{s} \frac{g_{io}}{4} [B_v(t) + \sum_{j=1}^{6} B_j \sin(q_{vj} t + Y_j) \quad (2)$$

where, subscript i=s for the Sun and i=m for the Moon; u and v are the zonal and meridional speed components, respectively, with u=U_0+GDMu, v=V_0+GDMv, U_0 and V_0 are respectively the first-mode speed of u and v, approximated to maintain the quasi-geostrophic balance among the pressure gradient force, Coriolis force, friction, and their acceleration (dU_0/dt and dV_0/dt) [47]. *GDMu* and *GDMv* are the zonal and meridional GDM components, as the second-mode speed of u and v, respectively; dissipation takes the form of "Rayleigh friction" that fits low-speed fluids like the atmosphere, oceans, and magma; k_f is the dissipation coefficient (s^{-1}); ρ, p, λ and φ are the density (kg m^{-3}), pressure (kg $m^{-1}s^{-2}$), geographical longitude and latitude of fluids, respectively;

Aj=[1,1, k_i, -k_i, k_i-k_i] B_j [-0.5, 0.5, -k_i , k_i, k_i], X_j [2λ+ϕ, 2λ-ϕ,λ+ϕ, λ-ϕ, λ-ϕ, λ+ϕ] and Y_j = [2λ+2ϕ, 2λ-2ϕ, λ+2ϕ, λ-2ϕ, λ-2ϕ, λ+2ϕ] are used for subscript j=1-6, respectively; B_v= [k_i^2-k_i^2 cos(2$f_{ir}t$)-1] sin[2$R_e^{-1}\int_0^t v dt$ +2ϕ] ; k_m=±18.3π/180 and k_s= ±23.45π/180 (+/- in the Northern/Southern Hemisphere), the obliquity of the orbital plane of the Moon and the Sun, respectively; q_{u1}=2(f_e-f_{ir}+C_u)+C_v; q_{u2}=2(f_e-f_{ir}+C_u)-C_v; q_{u3}=f_e-2f_{ir}+C_u+C_v; q_{u4}=f_e-2f_{ir}+C_u-C_v; q_{u5}=f_e+C_u+C_v; q_{u6}=f_e+C_u+C_v; q_{v1}=2(f_e-f_{ir}+C_u+C_v); q_{v2}=2(f_e-f_{ir}+C_u-C_v); q_{v3}=f_e-2f_{ir}+C_u+2C_v; q_{v4}=f_e-2f_{ir}+C_u -2C_v; q_{v5}=f_e+C_u-2C_v; q_{v6}=f_e+C_u+2C_v; q_{v7}=2f_e-2f_{ir}+2C_u; C_u = (tR_e COSϕ)$^{-1}\int_0^t$u dt and C_v = (tR_e)$^{-1}\int_0^t$v dt the longitude and latitude (divided by time t) for moving fluids at time t, respectively; Re=6,371,000, the Earth's radius (m); r_{om}=3.844×10^8 and r_{os}=1.496×10^{11}, the distance (m) between the centers of the Earth and the Moon and Sun, respectively; f_e=π/(12×3600), f_{mr}=2π/(29.5306×24×3600), and f_{sr}=2π/(365.2422×24×3600), the apparent angular velocity (s^{-1}) of the Earth's rotation, Moon's and Sun's revolution, respectively; g_{mo}=2$G_r$$M_m$$R_e$$r_{om}^{-3}$, g_{so}=2$G_r$$M_s$$R_e$$r_{os}^{-3}$, G_r =6.672X10^{-11}, the gravitational constant ($m^3kg^{-1}s^{-2}$); M_m= 7.348×10^{22} and M_s=1.989×10^{30}, the mass (kg) of the Moon and Sun, respectively.

For unit mass of fluids, the net meridional momentum (m/s), the net

zonal and meridional angular momentum divided by Earth's radius (m/s), and Earth's rotational contribution (%) were respectively computed as follows:

$$M_v = \frac{1}{\pi}\int_{-\pi/2}^{\pi/2} F(\phi)(V+v)cos\phi d\phi \quad (3)$$

$$MA_u = \frac{1}{R_e(\phi_2-\phi_1)}\int_{\phi_1}^{\phi_2}(U+u)F(\phi)(R_e+h)cos\phi d\phi \quad (4)$$

$$MA_v = \frac{1}{R_e(\phi_2-\phi_1)}\int_{\phi_1}^{\phi_2}(V+v)F(\phi)(R_e+h)cos\phi d\phi \quad (5)$$

$$F_{ec} = 100\times\frac{I_o}{f_e}\sum_{oceans}^{atmosphere}(U+u)M\int_{\phi_1}^{\phi_2}F(\phi)(R_e+h)cos\phi d\phi \quad (6)$$

where, I_o = 8.036×10^{37} kg m^2, Earth's moment of inertia; for the atmosphere, M=5.3×10^{18} kg and *h = 4,400 m, the mass and half thickness of an even-density atmosphere, respectively,* ϕ_1*= -π/2,* ϕ_2 *=π/2, and F(ϕ)=114.59cos ϕ (based on a 1° latitude resolution); for oceans, M = 1.4×10^{21} kg and h = -2,000 m, the mass and approximately half depth of oceans, respectively,* ϕ_1 *= -π/3,* ϕ_2 *= π/3, and F(ϕ) = 99.74cos ϕ (based on a 1° latitude resolution).*

GDM-induced Earth's rotation rate (s^{-1}) is:

$$f_{et}(t) = A_{nm}(t)/I_{ot}(t) \quad (7)$$

where, A_{nm} is the net zonal angular momentum (kg m^2/s) produced by the GDM of the fluids available relative to the rotating Earth at time t, computed from Equations (1) and (2); I_{ot} is the moment of inertia of Earth (kg m^2), derived as:

$$I_{ot} = 26\pi\rho_{eo}(t)R_t^5/175 \quad (8)$$

The radius (m) for a gaseous or a cooled Earth is:

$$R_t = \sqrt[3]{225M_e/[122\pi\rho_{eo}(t)]} \quad (9)$$

Earth's density changes vertically, was approximated to decrease exponentially from Earth's core where Earth's density is ρ_{eo}, and was fixed in a Taylor expansion as:

$$\rho_{et}(z) = \rho_{eo}(t)(1 - z/R_t + 0.4z^2/R_t^2 - z^3/R_t^3/6) \quad (10)$$

M_e = 5.9722×10^{24} kg, Earth's mass.

Climate changes may cause the irregular distribution of, for example, surface water via an ice-water phase change and may further alter Earth's rotation, obliquity, and inertia momentum. For the computation of these potential changes, the model (as depicted in Figure 6) was established using the conservation of angular momentum for Equations (11) and (12) and mass conservation for Equation (13), as follows:

$$I_o(f_c + f_e cos\Omega) = (I_o + \Delta I)[f_c + f_e\cos(\Omega + \Delta\Omega)] \quad (11)$$

$$I_o f_e = (I_o + \Delta I)(f_e + \Delta f_e) \quad (12)$$

$$2h_w\rho_w\cos(\phi_s+\phi_n)\sin(\phi_n-\phi_s) + \rho_i(h_s + h_n + h_s sin\phi_s - h_n sin\phi_n) = 0 \quad (13)$$

Changes in inertia momentum (ΔI, in kg m^2) were further solved as:

$$\Delta I = R_e\{[\rho_i\int_{\phi_n}^{\pi/2}\int_{R_e cos\emptyset}^{(R_e+h_n)cos\phi} + \rho_i\int_{-\pi/2}^{\phi_s}\int_{R_e cos\emptyset}^{(R_e+h_s)cos\emptyset} + \rho_w\int_{\phi_s}^{\phi_n}\int_{R_e cos\emptyset}^{(R_e+h_w)cos\emptyset}]\int_0^{2\pi} F(r,\theta,\phi)d\theta d\phi\, dr \quad (14)$$

where, ρ_i = 920 kgm^{-3} and ρ_w=1,000 kgm^{-3}, the density of ice and water, respectively; β = $-arctan\left(\frac{r}{R}cos\theta csc\phi\right)$, $F = rcos\phi\{r^2 + Rsin\phi sin\Omega\sec(\Omega-\beta)[Rsin\phi sin\Omega\sec(\Omega-\beta) - 2rcos\beta cos\theta]\}$. Additional parameters are described in Figure 6.

Using Ekman theory33, the westward transport flux of water produced by wind stress within a latitudinal cross section from y1 to y2 was summarized as [33].

$$F_{lux} = \int_{y_1}^{y_2}\frac{\rho_a C_D U_a v_a}{f\rho}dy \quad (15)$$

where, f = 1.458×10^{-4}×sin(y/R$_e$) (s^{-1}), the Coriolis parameter; ρa = 1.29 kg/m^3, the surface air density; ρ = 1025 kg/m^3, the water density; C_D = 0.0015, the larger sea surface drag coefficient; U_a and v$_a$, the surface wind speed and its meridional component, respectively.

Acknowledgement

During the period of 1997-2014 when I performed this study, I had partial facility supports from: 1) Drs. Dale Haidvogel and James Miller (Institute of Marine and Coastal Sciences, Rutgers, the State University of New Jersey, 2007− 2014); 2) Drs. Dake Chen, Jianhua Qian, and Naomi Naik (Lamont-Doherty Earth Observatory, Columbia University, 2001−2006); and 3) Profs. Chenglan Bao, Dayong Jiang and Jiping Cao, and my bosses Xuejia Song, Shimei Xie, and Zhanggui Wang (National Research Center for Marine Environmental Forecasts, 1997−2001). Specially thanks Drs. Dexing Wu, Xueen Chen and Xiaopei Lin (Physical Oceanography Laboratory, Ocean University of China) for paying publishing fees for papers [10-11].

References

1. Cheng M K, EanesRJ, Tapley BD (1992) Tidal deceleration of the Moon's mean motion. Geophysical Journal International 108: 401-409.
2. Ray R D, Eanes R J, Chao B F(1996) Detection of tidal dissipation in the solid earth by satellite tracking and altimetry. Nature 381: 595-597.
3. Egbert G D, Ray R D (2000) Significant dissipation of tidal energy in the deep ocean inferred from satellite altimeter data.

Nature 405: 775-778.
4. Miyazaki M (1958) A method for the harmonic analysis of tides, The Oceanogr Magazine 10: 91- 109.
5. Dronkers J J (1964) Tidal Computations in Rivers and Coastal Waters. North-Holland Publishing Company– Amsterdam DOI: 10.1126/science.146.3642.390
6. Parker B B (1984) Frictional Effects On The Tidal Dynamics Of A Shallow Estuary. The johns Hopkins University, Baltimore, MD 292p.
7. Fang G (1987) nonlinear effect of tidal friction, Acta Oceanologica Sinica 6:105-122.
8. Hunt J N, Jonhns B (1963) Currents induced by tides and waves, Tellus 15: 343-351.
9. Imasato N (1983) what is tide-induced residual current? J. of Physical Oceanogr 13: 1307-1317.
10. Zhiren Wang, Dexing Wu, Xuejia Song, Xueen Chen, Stephen Nicholls (2012) Sun-Moon Gravitation Induced Wave Characteristics and Climate Variation. J. Geophys. Res doi. org/10.1029/2011JD016967.
11. Wang Z, Lin X (2015) Astronomy and Climate-Earth System: Can Magma Motion under Sun-Moon Gravitation Contribute to Paleoclimatic Variations and Earth's Heat? Advances in Astronomy doi: 10.1155/2015/536829.
12. Wang Z (2016) Preliminary studies of climate-environment dynamics for our Climate Prediction and Environment,Outskirt Press ISBN 9781478779032, p 308.
13. Lau K M, Chan H (1986) The 40-50 day oscillation and the El Niño/Southern Oscillation: A new perspective, J. Atmo. Sci 67: 533-534.
14. Meehl G A (1987) The annual cycle and interannual variability in the tropical Pacific and Indian Ocean regions, Mon.Wea. Rev 115: 27-50.
15. Angell J K, Korshover J (1964) Quasi-biennial variations in temperature, total ozone, and tropopause height, J. Atmo. Sci 21: 479-492.
16. Kushnir Y (1994) Inter decadal variations in North Atlantic sea surface temperature and associated atmospheri conditions, J. Climate 7: 141-157.
17. Alley R B, Anandakrishnan S, Jung P (2001) Stochastic Resonance in the North Atlantic. Paleoceanography 16: 190-198.
18. Muller R A, MacDonald G J (1997) Spectrum of 100-kyr glacial cycle: orbital inclination, not eccentricity. Proc. Natl. Acad. Sci. USA 94: 8329-8334.
19. Raymo M E. Nisancioglu K (2003) The 41 kyr world: Milankovitch's other unsolved mystery. Paleoceanography doi.org/10.1029/2002PA000791.
20. Perigaud C M, Cassou C (2000) Importance of oceanic decadal trends and westerly wind bursts for forecasting El Niño. Geophys. Res. Lett 27: 389-392.
21. Wyrtki K (1975) El Niño-the dynamic response of the equatorial Pacific Ocean to atmospheric forcing. J. Phys Oceanogr 5: 572-584.
22. Jin F F (1997) An equatorial ocean recharge paradigm for ENSO, Part I: conceptual model. J Atmosph. Sc 54: 811-829.
23. Wang C (2001) A unified oscillator model for the El Niño-Southern Oscillation, J. Climate 14: 98-115.
24. Cane M A, Munnich M, Zebiak S E (1990) A Study of Self-Excited Oscillations of 609 the Tropical Ocean - Atmosphere System .1. Linear-Analysis. J. Atmos. Sci 47: 1562-1577.
25. Dake Chen, Mark A Cane, Alexey Kaplan, Stephen E Zebiak, Daji Huang (2004) Predictability of El Niño over the past 148 years, Nature 428: 733-736.
26. Moore A M, Kleeman R(1999) Stochastic forcing of ENSO by the intraseasonal oscillation, J. Clim 12: 1199-1220.
27. Crowley TJ (2000) Causes of Climate Change Over the Past 1000 Years. Science 289: 270-277.
28. J Jouzel, V Masson-Delmotte, O Cattani, G Dreyfus, S Falourd et al. (2007) Orbital and Millennial Antarctic Climate Variability over the Past 800,000 Years. Science, 317: 793-797.
29. 29. Lea D W (2004) The 100,000-Yr Cycle in Tropical SST, Greenhouse Forcing, and Climate Sensitivity. J. of Climate 17: 2170-2179.
30. Augustin L, Barbante C, Barnes PR, Barnola JM, Bigler M et al. (2004) Eight glacial cycles from an Antarctic ice core. Nature 429: 623-628.
31. Lambert F, Bigler M, Steffensen J P, Hutterli M, Fischer H (2012) Centennial mineral dust variability in high-resolution ice core data from Dome C, Antarctica. Climate of the Past 8: 609-623.
32. Wang Z, Wu D, Chen X, Qiao R (2012) ENSO Indices and Analysis, Adv. in Atmosph. Sci 30: 1491-1506.
33. Knauss J A (2005) An Introduction to Physical Oceanography, 2nd Ed., Waveland Press Inc pp309.
34. Cattermole P, Patrick M (1985) The Story of the Earth. Cambridge University Press ISBN 9780521262927.
35. Eggen OJ, Lynden B D, Sandage A R (1962) Evidence from the motions of old stars that the Galaxy collapsed. The Astrophysical Journal doi: 10.1086/147433.
36. Searle L, Zinn R (1978) Compositions of halo clusters and the formation of the galactic halo". The Astrophysical Journal 225: 357-379.
37. White S, Rees M (1978) Core condensation in heavy halos: a two-stage theory for galaxy formation and clustering. MNRAS 183: 341-358.
38. McPhaden M J, Zhang X (2009) Asymmetry in zonal phase propagation of ENSO sea surface temperature anomalies. Geophys. Res doi: 10.1029/2009GL 038774.
39. Thomson D J (1982) Spectrum estimation and harmonic analysis, Proc. IEEE 70: 1055-1096.
40. Gubbins D, MastersT G, Jacobs J A (1979) Thermal evolution of the Earth's core. Geophys. J.R.Astron.Soc 59: 57-99.
41. Pollack H N, Hurter S J, Johnson J R (1993) Heat flow from the Earth's interior: analysis of the global data set. Rev. Geophys 31: 267-280.
42. Hansen J, Nazarenko L, Ruedy R, Sato M, Willis J et al. (2005) Earth's energy imbalance: Confirmation and implications. Science 308: 1431-1435.
43. Foulger G R, Natland J H, Presnall D C, Anderson D L (2005) Plates, plumes, and paradigms: Geological Society of America Special Paper 388: 257-278.
44. Gerlach T M (2011) Volcanic versus anthropogenic carbon dioxide: Eos Trans. AGU 92 : 201-202.
45. Razumov SO, Spektor VB, Grigoriev M N (2014) Model of the Post-Cenozoic evolution of the cryolithozone of the shelf of the western part of the Laptev sea. Oceanology 54: 679-693.
46. Fisher RV, Heiken G, Hulen J (1998) Volcanoes, Crucibles of Change. Princeton University Press pp334.
47. Holton J R (1992) An Introduction to Dynamic Meteorology, 3rd Ed., Academic Press. 653 pp511.
48. Canup R M, Asphaug E Origin of the Moon in a giant impact near the end of the Earth's formation, Nature 412: 708-712.

49. Ćuk M, Stewart S T (2012) Making the Moon from a fast-spinning Earth: A giant impact followed by resonant despinning. Science 338: 1047-1052.

50. Williams D R (2007) Mercury Fact Sheet (http://nssdc.gsfc.nasa.gov/planetary) NASA.